PROPERTIES OF $^{192-190}Pb$; BEHAVIOUR OF THE VERY NEUTRON DEFICIENT EVEN LEAD ISOTOPES.

C. Roulet, G. Albouy, G. Auger,
J.H. Lagrange, M. Pautrat,
K.G. Rensfelt, H. Richel,
H. Sergolle, J. Vanhorenbeeck.

IPNO-PhN-78-12

Properties of $^{192-190}$Pb ; behaviour of the very neutron deficient even lead isotopes

C.Roulet, G.Albouy, G.Auger, J.M.Lagrange, M.Pautrat, K.G.Rensfelt[†], H.Richel[*], H.Sergolle, J.Vanhorenbeeck[**]

Institut de Physique Nucléaire, BP n°1, 91406 Orsay, France

Abstract.

The two very neutron-deficient isotopes of lead A≈190,192 have been produced and studied through the reaction $^{156-154}$Gd(^{40}Ar,4nγ)$^{192-190}$Pb. The identification of those nuclei was also studied by means of the two additional reactions : ^{182}W(^{16}O,6nγ)^{192}Pb and ^{156}Gd(^{40}Ar,6nγ)^{190}Pb. The pulsed ^{40}Ar beam available at ALICE (Orsay) enabled to record single γ spectra as well as four dimensional (energy-time) spectra corresponding to the correlation of two Ge(Li) detectors for different time windows. Tentative level-schemes are proposed. No significant deviation from the behaviour previously reported for the heavier isotopes (ref.1) is pointed out. The data are consistently reproduced within a 2 q.p formalism using an S.D.I residual interaction. However a slow decrease of the 2^+_1 level energy is observed which could be an indication of a weakly increasing collective trend when the number of neutron holes increases. Those experimental conclusions fairly agree with the theoretical predictions by F.Dickman and K.Dietrich (ref.2). As a matter of fact, the authors predict a spherical shape for the ground states and find a secondary prolate minimum of the deformation potential at low energy. But the latter is not well developped for A ≥ 184 suggesting a spherical behaviour for the heavier isotopes.

[†]Research Institute for physics, Stockholm, Sweden.

[*]Chercheur agréé U.L.B. Belgium

[**]Maître de recherche F.N.R.S. U.L.B. Belgium

I. Introduction.

The lead isotopes have been deeply studied from A=206 down to A=194. The lighter even isotopes studied through (heavy-ion,xn) reactions[1] exhibit a noticeable continuity in their behaviour. For instance, the high spin states are fairly well reproduced within a two-quasi particles formalism using an S.D.I residual interaction and a configuration-space built on the following neutron subshells : $\nu i13/2$, $\nu f7/2$, $\nu f5/2$, $\nu p3/2$, $\nu p1/2$ [3]. It was then interesting to extend the systematics of the even lead isotopes to lighter ones, the main aim being to investigate their behaviour according to nuclear deformation. The two isotopes with A=190 and 192 were totally unknown up to now. This paper deals with the experimental results obtained for them. A tentative level scheme based on γ-γ coincidences is proposed for each. A discussion is then made on the basis of a two-quasi particle formalism and a complete picture is given within that framework for all the known neutron-deficient lead isotopes.

II. Experimental procedure.

The experimental arrangement used in order to study the γ-rays following the compound nuclei de-excitation is very schematically represented in fig.1. A more complete description of the experimental set-up and the techniques used to sort the data can be found in ref.[4]. Two Ge(Li) detectors are used for γ-rays analysis (10% efficiency with respect to a 3"x3" NaI(Tl) detector, 2.7 keV FWHM at 1.33 MeV). Singles as well as coincidences spectra are recorded. A third detector, which essentially insists of a thin plastic scintillator, enables to refer the events to a zero-time taken from the beam burst itself. This beam detector, its characteristics and possibilities are described elsewhere[4,5]. Four dimensional events are recorded on magnetic tapes in list mode. They content the following information : $E\gamma_1 \otimes E\gamma_2 \otimes t_1 \otimes t_{21}$ where $E\gamma_1$ and $E\gamma_2$ are set for the two detectors respective energies, t_1 and t_{21} are the elapsed time values for the detected events in counter 1 referred to the beam pulse and in counter 2 referred to counter 1 respectively. An off-line analysis of those data using the ARIEL computer facilities (Ref.4) to 6)) enables to select and study prompt and delayed γ-γ coincidences and to obtain time-decay curves for the γ-rays of interest

as well. In parallel, prompt and delayed single spectra are recorded. Short-delayed events occuring between the beam-pulses in the 150 ns range as well as long-delayed events which are detected between macro-pulses in the ms range are recorded. For the investigation of lifetimes greater than the natural beam repetition time (~ 160 ns in the present experiment), a beam pulser is used. It can eliminate either 4 bursts out of 5 or 9 out of 10 (ref.5)).

III. Production and identification of the A=192, 190 lead residual nuclei.

For all the studied reactions, self-supporting 5 mg/cm^2 targets made of enriched material have been used (table 1). In order to check the (Ar,Gd) projectile-target couple for lead isotopes production and study, the following reaction has been studied : $^{158}Gd(^{40}Ar(190MeV),4n)^{194}Pb^*$. As it leads to a previously known isotope (ref.1 for instance), one could then get an estimation of the cross section of interest as well as informations concerning the quality of the spectra with respect to those obtained through $W(^{16}O,xn)$ reactions[1,7]. As it can be seen on figure 2, the major exit channel for the reaction above mentionned leads to ^{194}Pb and the peak to background ratios are similar to those obtained in previous studies using carbon, nitrogen or oxygen induced reactions. So then, the following reactions have been studied :

$$\begin{cases} ^{156}Gd(^{40}Ar(190MeV),4n)^{192}Pb \\ ^{154}Gd(^{40}Ar(195MeV),4n)^{190}Pb \end{cases}$$

The identification of the A=190, 192 lead products for which no line was known up to now has been carried out through three different approaches which are briefly discussed below.

i) Use of relative intensities of known decay-products transitions:

For each of the reactions induced by the ^{40}Ar beam onto $^{158-156-154}Gd$ targets, a prominent mass value is observed in the long-delayed γ spectra (A=194,192,190 respectively). In order to get a clue for the corresponding lead isotopes production, a systematic study of relative intensities for transitions between low-lying states has been carried out for the mercury daughter nuclei (figure 3 and tables 1, 2). For the test-experiment performed on ^{158}Gd, only the $2^+ \rightarrow 0^+$ transition is observed for the decay product

^{194}Hg. This clearly indicates that only the low spin states are fed in ^{194}Hg, coming from the low spin states in ^{194}Tl. The 7^+ isomeric state is not populated. The latter nucleus is therefore reached through the corresponding lead isotope ground state decay. The 4n channel consequently is the dominant one for this reaction. The same investigations have been considered for the two other reactions. Considering the measured values for the relative intensities of the first transition in $^{192-190}$Hg [8,9] in the case of a Tl ground state decay, one can conclude (tables 2,3) from our data that the exit channel is open in both cases. However, its relative width compared to the (p,3n) process significantly decreases with A.

ii) Use of different reactions leading to the same compound nucleus:

The following reactions were considered :

$$^{182}W(^{16}O\ (132\ MeV),6n)^{192}Pb$$

$$^{156}Gd(^{40}Ar(225\ MeV),6n)^{190}Pb$$

The new γ-lines, selected from the previous reactions study (present in the prompt and short-delayed spectra and not present in the radioactivity spectra) are compared to the ones observed in the two new reactions (tables 4,5).

iii) Use of coincidences between γ and internal conversion X rays :

The selected new-lines are then checked through X-γ coincidences techniques in order to get a Z-assignment. The results for ^{192}Pb can be seen in table 6 for instance. Excitation functions have not been extracted because of the target thickness used in order to be able to observe the residual nuclei at rest. The three sets of informations mentionned above led to the identification of two series of lines for A = 192 and 190 lead isotopes which are indicated in tables 4 and 5 respectively.

IV. Experimental results : tentative level schemes proposed for $^{192-190}$Pb.

The correlations between the two sets of γ-lines extracted from the delayed γ-spectra (fig.4) and respectively assigned to ^{192}Pb and ^{190}Pb are established through the analysis of the delayed γ-γ coincidences. The prompt

coincidences mainly exhibit the coincidences system arising from the ground state band of the targets inelastically excited by the argon projectile. On the contrary, the delayed coincidences matrix clearly shows the correlations between the lines selected from the single spectra analysis (see fig.5 for instance). This latter set of coincidences is almost totally smeared off in the prompt bidimensional spectrum. This is due to the important continuous background together with the inelastic excitation of the target ground band states.

IV.a. ^{192}Pb nucleus.

The results extracted from the delayed coincidences analysis for this nucleus are summarized in table 6. Three main features come out.

- All the lines exhibit coincidences with the characteristic lead XKα, XKβ transitions. This has been used for the Z-assignment previously discussed.
- A double coincidence peak is observed for $E\gamma \sim 502$ keV. This problem has been solved by using a complete bidimensional scanning of the region of interest[19]. Two lines very close in energy (501.7 keV and 503 keV) were pointed out.
- Two parallel cascades are observed (69, 191, 464, 503 keV and 599, 564 keV respectively). They reach a common cascade (501.7, 852 keV) leading to the ground state.

The order of the different transitions is deduced from the analysis of relative intensities of the corresponding γ-rays observed in the delayed spectra. The latter values include the efficiency corrections and take into account the conversion coefficients for the proposed multipolarities coming from the spin-parity assignment discussed below.

Discussion of the proposed level scheme, spin-parity assignments:

Multipolarities have not been directly deduced for the observed transitions. As a matter of fact, all the lines exhibit a long-lived time distribution ($T1/2 \simeq 800$ ns) and the target structure (h.e.p.) is characterized by a short relaxation time. These two features lead to a strong loss of alignment for the nuclear spins. Therefore, angular distribution patterns

would appear almost isotropic. The proposed multipolarities and the related spin-parity assignment is derivated through a set of four arguments.

* E1 multipolarity assignment for the 69 keV transition:

According to the relative intensity observed in the delayed coincidences spectra for the 69 keV line, only the E1 multipolarity can be expected. Other possibilities such as M1, E2 or M2 would lead to very weak γ-ray intensities due to the very greater corresponding α_T conversion coefficients (see table 7 for numerical values).

* Connection of the 69 keV line with the $10^+ \xrightarrow{E1} 9^-$ transition:

If one considers the expected energy values for the $10^+ \xrightarrow{E1} 9^-$ and $5^- \xrightarrow{E1} 4^+$ transitions from the systematics on heavier even lead isotopes[1], only the former can be connected to the observed 69 keV line. As a matter of fact, the predictions are 500 keV and 80 keV respectively. Moreover, the experimental results which come from the delayed coincidences are in agreement with this assignment. If the 69 keV γ-ray was related to the $5^- \xrightarrow{E1} 4^+$ transition the 5^- state should have been characterized by an half-life in the hundred nanoseconds range like in heavier isotopes. Therefore the set of coincidences with the 191 keV and 464 keV would have vanished.

* Competitive decay of the isomeric $(\nu i13/2)^{-2}_{10^+}$ state through E1 and E2 transitions:

As it will be discussed in the next section dealing with the interpretation of the levels which are pointed out in the present work, the excited states for neutron deficient isotopes of lead may be understood within a two quasi-particle formalism at least for the higher spins. The configuration space is limited to the five following neutron subshells : p1/2, p3/2, f5/2, f7/2 and i13/2. Then the triplet 12^+, 10^+, 8^+ is described by the only pure configuration $(\nu i13/2)^{-2}$ (ref.3). Using such a basis, the energy splitting between the different members is expected to be weak ($\simeq$ 60 keV). This has already been checked experimentally (^{206}Pb (ref.20) and ^{198}Pb (ref.21) for instance). According to those energy predictions, one can expect both $12^+ \xrightarrow{E2} 10^+$ and $10^+ \xrightarrow{E2} 8^+$ transitions to be isomeric. For the heavier isotopes ($194 \leq A \leq 200$), the 12^+ and 10^+ were found experimentally whereas the

8^+ level is not observed yet. This can be understood when considering the great energy value measured for the $10^+ \xrightarrow{E1} 9^-$ transition which makes this transition much more likely than the $10^+ \xrightarrow{E2} 8^+$ one. On the contrary, for ^{192}Pb, the energies are very close each other for both transitions which become then competitive ($10^+ \xrightarrow[69\,keV]{E1} 9^-$, $10^+ \xrightarrow[64\,keV]{E2} 8^+$). Therefore one can expect a decay for the $(vi13/2)^{-2}_{10^+}$ isomeric state through two parallel cascades: (10^+, 8^+, 6^+, 4^+ and 10^+, 9^-, 7^-, 5^-, 4^+). A rough calculation has been carried out in order to check the whole consistency of the proposed level scheme (fig.6) and in particular the corresponding spin-assignment. The branching ratio for a given state decay through E1 and E2 transitions may be expressed as :

$$\frac{I(E1)}{I(E2)} = \frac{B(E1)}{B(E2)} \times \frac{(1+\alpha_T)_{E1}(E1)^3}{(1+\alpha_T)_{E2}(E2)^5} \times \frac{0.435}{0.565} \qquad (1)$$

where the energies are understood in keV and B(E1,E2) in e^2fm^2, e^2fm^4 respectively. An order of magnitude can be got for B(E1) and B(E2) values when considering the corresponding experimental values for $12^+ \xrightarrow{E2} 10^+$ and $5^- \xrightarrow{E1} 4^+$ transitions in the heavier isotopes. From the known $B(E2)(12^+ \to 10^+)$ [20,21] one gets an average value $B(E2) \sim 60\ e^2fm^4$. For the $10^+ \xrightarrow{E2} 8^+$ transition a correction only due to geometrical factors leads to the average value : $B(E2)(10^+ \to 8^+) \sim 20\ e^2fm^4$. For the E1 transition, as nothing is known up to now about the $10^+ \to 9^-$ case, the results concerning the $5^- \xrightarrow{E1} 4^+$ transition have been used. An average value is taken from the isotopes with $194 \leq A \leq 200$ (ref.23) : $B(E1) \simeq 5\ 10^{-6} e^2fm^2$. The same hindrance factor compared to the Weisskopf estimation $(B(E1)_{sp} = 2.2\ e^2fm^2)$ is assumed for the $10^+ \xrightarrow{E1} 9^-$ transition. With those two estimations, which are kept for all the transitions studied, an order of magnitude is deduced for the γ-branching ratios for some excited states (table 8). From the obtained values, one can first conclude that the existence of two separate cascades for the 10^+ state decay is very well accounted for. The crossing transitions between the cascades of different parity is very unlikely (a doubtful prediction is obtained for the 7^- case however). Moreover, the different behaviour for A=194 and A=192 is clearly shown (respective branching ratios : 29.2 and 2.1).

* Evidence for high-spin and long-lived isomeric states:

All the delayed lines which are assigned to ^{192}Pb exhibit a similar

time-decay curve with a prominent long-lived component (T1/2 ≈ 875±200 ns). (fig.7). This gives evidence for one high-spin isomeric state at least. As a matter of fact, the T1/2(12^+) value expected from the systematics must be around 500 ns. In the present case where both 12^+ and 10^+ states certainly are isomeric, the observed behaviour for the time-decay curves is very likely due to the influence of the two corresponding half-lives. The recorded data do not provide statistics enough to be able to analyze in more details the time distributions versus the two possible components.

In conclusion, this set of arguments together with what one could expect from the systematics extrapolation allow us to propose the level scheme shown on fig.6. These arguments are not strong arguments but they are all consistent as a whole. It must be remembered that angular distributions measurement would be very difficult to perform according to the long-lived high spin isomeric states and the h.c.p. target structure. In the same way, on line conversion electrons study would also be rather uneasy according to the target thickness problems and the poor production yield related to the weak cross section.

IV.b. ^{190}Pb nucleus.

For this nucleus, the delayed γ-γ coincidences analysis was much more uneasy according to the very weak statistics. The competition with other exit channels such as (p,3n) and even fission which may begin to play a significant role leads to a weak cross section for the 4n outgoing channel of interest for the ^{190}Pb production. Table 9 summarizes the coincidences observed for the set of lines selected from the analysis of the single spectra and some typical spectrum is displayed in figure 8. From these results a cascade of coincident transitions is clearly pointed out. The two first levels (773 keV and 1280 keV) are deduced from the relative intensities analysis and are in very good agreement with the systematics predictions. The order of the different transitions mentionned in figure 9 is based on the same arguments. It has not been possible however to make a definitive choice for the respective order of the 454 keV and 540 keV according to the comparable corresponding intensities.

Whereas the two first levels may be interpreted according to the systematics prediction and the experimental results, no information has

been obtained about the spin and parity for the higher energy levels. The ambiguities coming from the double coincidences-peaks together with the lack of informations about the multipolarities do not allow us to describe in more details the levels which are pointed out. The double coincidences are still open problems. It has not been possible to resolve the complex structures even with a bidimensional scanning of the data. The 338 keV double coincidence may certainly be trusted whereas the 507 keV one may be likely due to some slight admixture of the 511 keV annihilation peak.

In conclusion, two main features come out for this nucleus. According to the present data, only one cascade of five coincident transitions is pointed out and all the lines are delayed and managed by the same long half-life (about 1 μs). The energy of the highest level found here (2611 keV) is fairly close to the one observed for the 10^+ and 9^- states in ^{192}Pb. However it is not possible to know which one of those states is reached and consequently whether the observed decay occurs through the $9^-\rightarrow7^-\rightarrow5^-\rightarrow4^+\rightarrow2^+\rightarrow0^+$ cascade like in the heavier isotopes ($194 \leq A \leq 200$) or another sequence which would give rise to a new and interesting behaviour.

V. Discussion

Experimental data are now available over a wide range of neutron-deficient even isotopes of lead ($190 \leq A \leq 206$). It is then very convenient to include the discussion on the two new isotopes within a more general survey of all the isotopes. Fig.10 shows the experimental systematics for two sets of levels (respectively 2^+, 4^+, 10^+, 12^+ and 5^-,7^-,9^-) which are observed for almost all the isotopes. Three general comments arise :

- The levels which are pointed out in the present work for ^{192}Pb (8^+,6^+ apart because unknown for the heavier isotopes), as well as the two first levels observed for the ^{190}Pb nucleus, nicely fit the general systematics.

- The energy of the 10^+ and 12^+ levels regularly decreases with A. However, it becomes more or less stationary for the lightest isotopes.

- The energy of the two low-lying levels 2^+ and 4^+ increases down to A=196 about and then slightly decreases with A. This could suggest a slow evolution towards a more collective nature for those states.

In addition to those general trends, a particular aspect has to be discussed for $^{190-192}Pb$. It is indeed very interesting to try to understand the different behaviour observed for these two isotopes for which either two decaying cascades (^{192}Pb), or only one (^{190}Pb) like for the heavier masses, are observed. In the latter case where no experimental spin-parity assignment is available at present, it is then important to investigate the various predictions.

V.a. Extension of the calculations within the Tamm Dancoff approximation (T.D.2) to A = 190,192.

The results previously obtained for the heavier isotopes ($194 \leq A \leq 200$) were analysed through a two quasi-particle calculation (T.D.2). Various residual interactions were used such as the surface delta interaction (S.D.I) and a central gaussian force (C.G.F) [1,2,3]. The basis was restricted to the five neutron subshells p1/2, p3/2, f5/2, f7/2, i13/2. The general trend of the high spin states, the configurations of which are expected fairly pure within that basis, is well accounted for when using the S.D.I interaction ($4\pi G = .165$). The 12^+, 10^+ states are then described by the only $(\nu i13/2)^{-2}$ configuration and this has been experimentally confirmed by g-factor measurements results[24]. On the other hand, the low-lying 2^+, 4^+ levels are not reproduced and located much too high in energy. Moreover, the trend is not reproduced because, within the TD2 approximation, the 2^+ energy is expected to increase when the isotopes become lighter. This is partly due to the overestimated gap energy which pushes down the 0^+ ground state. In addition this kind of calculation together with the residual interaction itself are not very convenient to account for such states for which the admixture of many configurations may occur.

The two new isotopes are investigated through the same treatment (fig.11). The consistency of the SDI interaction with the TD2 approximation is checked using a spectral distribution calculation in the subspaces defined by their number of quasi-particles K [25]. The overlap of the different subspaces which strongly depends on the residual interaction is significantly weaker for the SDI and pairing interactions. For the latters, the overlap with quasi-particle subspaces with $K \geq 4$ is weak below 2.6 MeV. The SDI interaction suits then very well the TD2 approximation.

Fig.11 shows the various predictions obtained within the TD2 approximation using the SDI interaction. Column 1 corresponds to the experimental situation. Two different basis are considered :

- The first one is built on the five neutron subshells previously mentionned for which the strength ($4\pi G$) is set to 0.165 to account for the experimental 10^+ level (column 2).
- The second one includes the neutron 1h9/2 orbit. This subshell is more bound than the 2f7/2 orbital but is expected to come closer to and even cross it for very deficient isotopes[26]. It must then begin to play some role for A≈192, 190. The strength is then re-adjusted to 0.145.

For A = 192, the 8^+ and 9^- states are expected very close to each other and very close to the 10^+ level. This is in perfect agreement with the two observed parallel cascades. For A = 190, the relative order of 9^- and 10^+ states is reversed in comparison with heavier isotopes. This provides some possible interpretation of the only cascade experimentally observed. Using the same SDI strength as for A ≈ 192, the 12^+, 10^+, 8^+ triplet position is expected to lay around the 2.61 MeV level which is experimentally pointed out. As the $10^+ \to 8^+$ transition cannot be observed according to its too low energy, the experimental level could be considered as the 8^+ one. Two different decaying cascades might be considered :

- $8^+ \overset{E1}{\to} 7^- \to 5^-(6^+) \to 4^+ \to 2^+ \to 0^+$
- $8^+ \overset{E2}{\to} 6^+ \to 5^- \to 4^+ \to 2^+ \to 0^+$

depending on the relative E1 and E2 probability for the 8^+ state decay. No significant improvement is obtained when using the six subshells basis despite a more realistic prediction of the 5^-, 4^+ states energy spacing.

Considering the whole systematics ($190 \lesssim A \lesssim 206$), the 12^+, 10^+, 8^+ are well described within this formalism using the same strength (0.165) and the same five subshells. The 10^+, 12^+ levels energy nicely follows the general trend of the $(vi13/2)^{-2}$ configuration (fig.12). The evolution of the 7^- and 9^- states the main configuration of which is $(vi13/2^{-1}, f5/2^{-1})$ also is well accounted for. The low-lying levels (2^+,4^+,5^-) are too high compared to the experimental data and the discrepancy is still more pro-

nounced for the lighter isotopes. The quadrupolar part of the interaction has been artificially enhanced by increasing the strength. The interaction is then readjusted by subtracting a pairing component. The pairing part is set in order to fit the 2^+ state and the intensity balance between the two parts of the interaction is adjusted on the 10^+ energy (fig.11 column 4 and 5). Of course, the low-lying levels are better reproduced but the prediction of the relative order of the high spin states is no longer accounted for. Moreover this procedure is not satisfactory according to the pairing strength which is clearly A-dependent. Whereas the high spin states are fairly well described within the TD2 formalism using the SDI interaction even for very light isotopes, the low spin states appear to be much more complex and call for refinements at least and even for different approaches.

V.b. Admixture of configurations involving a great number of quasi particles

The strong discrepancy between the experimental 2^+ systematics and the predictions from the TD2 approximation using the SDI interaction may arise from two different reasons.

- Very many low spin states very close in energy may occur. Then, the use of a more realistic nucleon-nucleon interaction might lead to more coherent (collective) states with a significant decrease of the energy.
- One could think of the subspaces with a great number of quasi particles (K>2) which are expected to play a significant role for the low energy levels[25].

Some recent calculations[28,29] based on the spectral distribution method[27] were applied to subspaces where the generalized seniority is fixed. In the case of even neutron-deficient isotopes of lead, it is shown that states with a generalized seniority value up to 6 must be included to reproduce the trend of the first 2^+ state (fig.13). This extension of the calculations has then to be done first and before any further investigation towards more realistic interactions. For the first 2^+ state which is the only state one can calculate through the present method, figure 13 shows the comparison between the data, the predictions from TD2 and from the new treatment. The latter involves K=2,4,6 subspaces. The general trend (relative values) isbetter reproduced. This indicates that the admixture of K=2,4,6 subspaces might be

a major reason for the 2^+ energy decrease observed with A down to 190.

V.c. Possible axial deformation for low-lying states in the light isotopes of lead

A general investigation by Dickmann and Dietrich[2] was carried out for light even Pt, Hg and Pb isotopes. Whereas the low energy spectra for the neutron deficient mercury isotopes are interpreted through a mixing between spherical and deformed states, the lead isotopes are expected to show spherical ground states. In addition, the deformation energy curves exhibit a secondary prolate minimum (β=.19) at low energy (see for instance ref.2, fig.3). However, the latter is not well developped and is not clear for A>188. Using different pairing forces (with a strong or weak isospin dependence), a significant prolate minimum is not expected to occur before A=184 or lower respectively.

On the other hand, calculations using the minimization of an effective deformation energy were done by May et al.[30]. For the lower states (2^+, 4^+), an oblate minimum is expected which lies below the prolate one. Moreover, a shape transition towards a prolate deformation is predicted for higher spins (I=8 for A=188). However the 2^+ energy happens to be significantly larger than the experimental one (1.4 MeV in the BCS treatment, 1.72 MeV with the Q-projection approach for A=192) and further investigations are needed to improve the agreement.

Forgetting the discrepancy about the nature (prolate/oblate) of the expected deformation which is still an open problem, the two calculations seem to lead to a likely axial deformation for low spin states in neutron-deficient lead isotopes but not before A=186 at least.

According to the data available up to now for neutron-deficient isotopes of lead and within the framework of the discussion developped above, one can extract the following conclusions. Down to eighteen holes in the N=126 closed shell, the isotopes of lead are surprisingly well described within a two-quasi particle formalism using the very simple SDI interaction (same strength 4xG=0.165) as far as one is concerned with high spin yrast states. The general trend of the low-lying states such as the 2^+,4^+ levels does not lead to a clear evidence for nuclear axial deformation. The 2^+ energy decrease may be understood either by including the admixture of 4 and

6 quasi-particles subspaces which seem to play a role even for low energies or by a nature more and more coherent (increasing configuration mixing) which could be accounted for by choosing a more realistic interaction. It is then more likely to understand those nuclei as spherical nuclei, well described within shell model calculation for the high spin states with simple configuration involving spherical orbits and which low lying states trends may be understood by a slight enhancement of the collective character when A decreases.

References

1) M.Pautrat, G.Albouy, J.C.David, J.M.Lagrange, N.Poffé, C.Roulet, H.Sergolle, J.Vanhorenbeeck, Nucl. Phys. A201 (1973) 449

2) F.Dickmann, K.Dietrich, Zeitschrift für Physik 271 (1974) 417

3) G.Albouy, J.M.Lagrange, M.Pautrat, C.Roulet, H.Sergolle, J.Vanhorenbeeck, Phys. Scripta Vol.6 (1972) 219

4) C.Roulet, Thesis Orsay (1975)

5) C.Roulet, G.Albouy, G.Auger, M.P.Bourgarel, J.C.David, J.M.Lagrange, B.Monsanglant, M.Pautrat, H.Richel, H.Sergolle and J.Vanhorenbeeck, NIM 125 (1975) 29

6) G.Albouy, J.C.David, J.M.Lagrange, M.Pautrat, C.Roulet, H.Sergolle, J.Vanhorenbeeck, Nucl. Inst. Meth. 113 (1973) 509

7) H.Richel, G.Albouy, G.Auger, J.M.Lagrange, M.Pautrat, C.Roulet, H.Sergolle, J.Vanhorenbeeck, Zeit. für Phys. A284 (1978) 425

8) J.Vandlik, T.B.Vandlik, N.G.Zaitseva, I.Mahunka, M.Mahunka, Z.Maté, K.H.Tinov, T.Fenyes (Kiev 1972, p.158)

9) J.Vandlik, N.G.Zaitseva, Z.Maté, I.Mahunka, M.Mahunka, T.Fenyes, Isvestia Physics vol.34 n°8 (1970) 1656

10) O.Lönsjö, G.B.Hagemann, Nucl. Phys. 88 (1966) 624

11) H.Beuscher, W.F.Davidson, R.M.Lieder, A.Neskakis, C.Mayer-Böricke, Phys. Rev. Lett. Vol.32 n°15 (1974) 843

12) P.Kilcher, Nucl. Phys. A118 (1968) 628

13) M.Lederer, J.M.Hollander, I.Perlmann, Table of Isotopes J.Wiley and Son New York (1967)

14) M.Finger, R.Foucher, J.P.Husson, J.Jastrzebski, A.Johnson, G.Astner, B.A.Erdal, A.Kjelberg, P.Patzelt, A.Hoglund, S.G.Malmskog, R.Henck, Nucl. Phys. A188 (1972) 369

15) J.Vandlik, T.B.Vandlik, N.G.Zaitseva, Z.Maté, I.Mahunka, M.Mahunka, K.H.Tirov, T.Fenyes, V.I.Fominikh, Isvestia Physics Vol.38 n°4 (1974) 689

16) J.Vandlik, N.G.Zaitseva, Z.Maté, I.Mahunka, X.Tyrroff, T.Fenyes, Isvestia Physics Vol.38 n°4 (1974) 695

17) J.O.Newton, F.S.Stephens, R.M.Diamond, Nucl. Phys. A236 (1974) 225

18) C.Vieu, J.S.Dionisio, Communication to the Topical Conference on Problems of Vibrational Nuclei (Zagreb, September 1974)

19) R.Jezequel, R.Sellem, "Sortie sur traceur digital d'histogrammes multidimensionnels" Internal Report (IPN Orsay) 1969

20) K.Nakai, E.Herskind, J.Blomqvist, A.Filevich, K.G.Rensfelt, J.Sztarkier, I.Bergström, S.Nagamiya, Nucl. Phys. A189 (1972) 526

21) G.Albouy, G.Auger, J.M.Lagrange, M.Pautrat, H.Richel, C.Roulet, H.Sergolle, J.Vanhorenbeeck, to be published in Nucl. Phys.

22) R.S.Hager, E.C.Seltzer, Nucl. Data A4 (1968) 1

23) G.Albouy, J.M.Lagrange, M.Pautrat, J.M.Rimbert, C.Roulet, H.Sergolle, J.Vanhorenbeeck, H.Abou-Leila, Le Journal de Physique Tome 33 (1972) 835

24) C.Roulet, G.Albouy, G.Auger, J.M.Lagrange, M.Pautrat, K.G.Rensfelt, H.Richel, H.Sergolle, J.Vanhorenbeeck, Nucl. Phys. A285 (1977) 156

25) G.Auger, V.R.Manfredi, Le Journal de Physique Colloque C5 Tome 36 (1975) p C5.91

26) C.J.Veje, Mat. Fys. Medd. Dan. Vid. Selsk. 35 n°1 (1966)

27) J.B.French, Nucl. Structure (North Holland Publ. Comp.) Amsterdam (1967)

28) S.Spitz, Thesis U.L.B. Brussel (1974)

29) C.Quesne and S.Spitz, to be published

30) F.R.May, V.V.Pashkevich, S.Frauendorf, JINR Report P4 10173 Dubna (1976) and Phys. Lett. 68B n°2 (1977) 113.

31) S.Spitz et al., to appear in Ann. of Physics.

Figure captions

Fig.1. Schematic view of the experimental set up and measured quantities.

Fig.2. Delayed γ-spectrum recorded for the reaction ^{40}Ar(190 MeV)+^{158}Gd.

Fig.3. Comparison of relative probabilities for the (p,3n) and (4n) exit channels through the study of the relative intensities corresponding to transitions between low-lying states in the decay mercury isotopes (A=194-192-190). See tables 2 and 3 for related numbers.

Fig.4. Delayed γ-spectra recorded for the reactions $^{156}Gd+^{40}Ar$(190 MeV)(a) $^{154}Gd+^{40}Ar$(195 MeV)(b).

Fig.5. Some selected delayed coincidences spectra for ^{192}Pb. Gates on the doublet 501.7 keV+ 503 keV, on 191 keV and 464 keV.

Fig.6. Proposed level scheme for ^{192}Pb.

Fig.7. Time decay curves for some transitions assigned to ^{192}Pb. The start pulse is in phase with the beam burst. The stop pulse is respectively provided by the 501.7+503 keV doublet (a), the 464 keV and 852 keV lines (b and c). A beam pulser was used (new beam repetition time : 790 ns . Each point corresponds to a stop summed over 14 channels which correspond to 80 ns).

Fig.8. Delayed coincidences for ^{190}Pb. Gate on 454 keV.

Fig.9. Tentative level scheme proposed for ^{190}Pb. The dashed lines correspond to the two possibilities for the respective order of the 454 keV and 540 keV transitions.

Fig.10. Experimental systematics of energy levels for even lead isotopes ($190 \lesssim A \lesssim 206$).

Fig.11. Theoretical predictions obtained for $^{190-192}Pb$ through a two quasi-particle calculation using an SDI residual interaction.

Fig.12. A-dependence of some two quasi-particle configuration energies. The curves correspond to independent quasi-particle energies (E(j,j') = E(j)+E(j')).

Fig.13. A-dependence of the first 2^+ level in lead isotopes. Comparison with the predictions made within the TD2 approximation and a calculation by Spitz et al. including states characterized by a great number of quasi-particles.

Tables

Target	Thickness mg/cm^2	Isotopic abundance %						
		152	154	155	156	157	158	160
Gd^{158}	5	<0.1	<0.1	0.96	1.7	3.56	92	1.82
Gd^{156}	5	<0.05	0.13	1.99	93.58	2.57	1.27	0.46
Gd^{154}	5	<0.01	93.35	0.18	0.10	0.04	0.02	0.01

Table 1. Gadolinium targets. Mass analysis

Energy (keV) transition	Relative intensity	
	This work	Ref.8)
422.8 $2^+ \rightarrow 0^+$	100	100
635.1 $4^+ \rightarrow 2^+$	31(5)	68
745.1 $6^+ \rightarrow 4^+$	13(3)	24

Table 2. Relative intensities for transitions between low-lying states in ^{192}Hg.

Energy (keV) transition	Relative intensity	
	This work	Ref.9)
416.0 $2^+ \rightarrow 0^+$	100	100
625.3 $4^+ \rightarrow 2^+$	46(5)	78(9)
730.9 $6^+ \rightarrow 4^+$	20(4)	49(9)

Table 3. Relative intensities for transitions between low-lying states in ^{190}Hg.

Table 4. ^{192}Pb lines identification. The table shows the comparison between the prompt, delayed and radioactivity spectra for the Ar induced reaction on ^{156}Gd and the delayed spectrum for the oxygen induced reaction on ^{182}W as well.

\+ is for a sure evidence.

I is for a incertain evidence.

ε is for a weak evidence.

a. Ref.10. b. Ref.11. c. Ref.8. d. Ref.12.
e. Ref.13. f. Ref.14. g. Ref.15. h. Ref.16.
i. Ref.17. j. Ref.18. k. This work.

Table 5. ^{190}Pb lines identification. The table shows the comparison between the prompt, delayed and radioactivity spectra for the Ar(195 MeV) induced reaction on ^{154}Gd and the delayed spectrum for the ^{40}Ar(225 MeV) induced reaction on ^{156}Gd. +, I, ε have the same meaning as mentionned in table 4.

a. Ref.10. b. Ref.17. c. Ref.16. d. Ref.12.
e. Ref.14. f. Ref.9. g. Ref.11. h. This work.

Energy (keV)	^{40}Ar (190 MeV) + ^{156}Gd			Identification		Ref.	^{16}O(152 MeV)+^{182}W
	Prompt	Short-delayed	Long-delayed				delayed
42.7	+	ε		XKα Gd			
48.9	+	ε		XKβ Gd			
69	I	+		^{192}Pb		k	ε
70.1		+	+	XKα Hg			
72.1		+	+	XKα Tl			
74.2	+	+		XKα Pb			+
80.7		+	+	XKβ Hg			
83.0		+	+	XKβ Tl			
85.4	+	+		XKβ Pb			+
8₀.36	+	ε		$2^+ \rightarrow 0^+$	^{156}Gd	a	
123.1	+			$2^+ \rightarrow 0^+$	^{158}Gd	a	
133		I	+	$7^- \rightarrow 5^-$	^{192}Hg	b	
157.2		+	+	$(0,1)^- \rightarrow 1^-$	^{192}Au	d	
163		+	+				
173.8		+	+	$7^- \rightarrow 6^+$	^{192}Hg	b	
181.94	+	ε		$4^+ \rightarrow 2^+$	^{158}Gd	e	
191	+	+		^{192}Pb		k	ε
199.19	+	+	+	$4^+ \rightarrow 2^+$	^{156}Gd partly	a	
250		+	+				
252.9		+	+		^{193}Au	h	
258		+	+		^{193}Au	j	
274.4		+	+	$(3/2^-) \rightarrow (1/2^-)$	^{193}Hg	g	
274.8		+	+	$1^+ \rightarrow (1,2)^-$	^{192}Au	d	
295.9		+	+	$2^{1+} \rightarrow 2^+$	^{192}Pt+^{193}Pt	f	
296.3	+			$6^+ \rightarrow 4^+$	^{156}Gd	a	
306.5		+	+	$1^+ \rightarrow 1^-$	^{192}Au	d	
308.5		+	+	$3^+ \rightarrow 2^{1+}$	^{192}Pt	f	
316.5		+	+	$2^+ \rightarrow 0^+$	^{192}Pt	f	
324		+	+	$(3/2^-) \rightarrow 3/2^-$	^{193}Hg	g	
327		+	+		^{193}Hg	h	
365	ε	+	+		^{193}Tl	i	
382	+	+	+	partly $8^+ \rightarrow 6^+$	^{156}Gd	a	
394		+	+		^{193}Au	j	
422.8		+	+	$2^+ \rightarrow 0^+$	^{192}Hg	b	
451	+			$10^+ \rightarrow 8^+$	^{156}Gd	a	
464	+	+		^{192}Pb		k	+
501.7	+	+		^{192}Pb		k	+
503	+	+		^{192}Pb		k	+
511	+	+	+	annihilation (e^+e^-)			
556		ε	+				
564	+	+		^{192}Pb		j	+
552			+				
599	+	+		^{192}Pb		j	+
612.4		ε	+	$2^{1+} \rightarrow 0^+$	^{192}Pt	f	
635.1		+	+	$4^+ \rightarrow 2^+$	^{192}Hg	b	
690		+		$0^{1+} \rightarrow 0^+$	^{72}Ge (n,n') ^{192}Hg	c	
691		(+)	+				
745.4		+	+	$6^+ \rightarrow 4^+$	^{192}Hg	b	
786.6		+	+	$5^- \rightarrow 4^+$	^{192}Hg	b	
811			+				
838		+	+				
848	+						
852	+	+		^{192}Pb		k	+
914		ε	+		^{193}Au	j	
1062	+				^{156}Gd	a	
1113		ε	+		^{192}Hg	c	
1274		+	+				
1304		+	+				

TABLE 4

TABLE 5

Energy (keV)	^{40}Ar (195 MeV) + ^{156}Gd			Identification	Ref.	$^{40}Ar(225\,MeV)+^{156}Gd$ delayed
	Prompt	Short-delayed	Long-delayed			
48	+			XKβ Gd		
66.2		+	+	XKα Pt		
68.2		+	+	XKα Au		
70.1		+	+	XKα Hg		
72.1		+	+	XKα Tl		
74.2	+	+		XKα Pb		
76.1		+	+	XKβ Pt		
78.3		+	+	XKβ Au		
80.7		+	+	XKβ Hg		
83.0		+	+	XKβ Tl		
85.4	+	+		XKβ Pb		
88.96	+			$2^+ \rightarrow 0^+$ ^{156}Gd	a)	
123.07	+	(+)		$2^+ \rightarrow 0^+$ ^{154}Gd	a)	
135	+			$2^+ \& 0^+ 0$ ^{154}Gd	a)	
142.7		+	+	$(1^+ \rightarrow 1,2^-)$ ^{199}Au	d)	
171.5		+	+	$1^- \rightarrow 1^-$ ^{198}Au	d)	
196.6		+	+	$7^- \rightarrow 5^-$ ^{199}Hg	f,g)	
199.19	+			$4^+ \rightarrow 2^+$ ^{154}Gd	a)	
215.6		+	+	^{197}Hg	c)	
232.1	+			$4^+ \& 2^+ 0$ ^{154}Gd	a)	
248.1	+			$4^+ \rightarrow 2^+$ ^{154}Gd	a)	
250		+	+	radioactivity ^{191}Au	c)	
252.6		+	+	^{191}Hg	c)	
264.7		+	+	^{191}Au	c)	
274.1		+	+	^{193}Hg	c)	
281.8		+	+	partly ^{193}Hg	c)	
284.4		+	+	^{193}Hg	c)	
296.8		+	+	$2^+ \rightarrow 0^+$ ^{198}Pt	e)	
296.5	+			$4^+ \rightarrow 4^+$ ^{156}Gd	a)	
302.0		+	+	$2^{+*} \rightarrow 2^+$ ^{198}Pt	e)	
305.0		+	+	$7^- \rightarrow 6^+$ ^{199}Hg	f,g)	
318.3	+			$6^+ \& 4^+ 0$ ^{156}Gd	a)	
319.3		+	+	$3^{-*} \rightarrow 2^+$ ^{198}Pt	e)	
325.6		+	+	$^{193}Hg+(13/2^- \rightarrow 11/2^-)$ ^{193}Tl	b)	
335.9		+	+	^{193}Hg	c)	
358	+	+		^{198}Pt	b)	+
346.9	+			$6^+ \rightarrow 4^+$ ^{154}Gd	a)	
372	+			(^{155}Gd)	i)	
374.3		+	+	^{197}Hg	c)	
378.1		+	+	^{193}Hg	c)	
378.7		+	+	^{193}Au	c)	
387.6		+	+	$11/2^- \rightarrow 9/2^-$ ^{193}Tl	b)	
405.0		+	+	$15/2^- \rightarrow 13/2^-$ ^{193}Tl	b)	
416		+	+	$4^+ \rightarrow 2^+$ ^{199}Hg	f,g)	
420.3		+	+	partly ^{193}Au	c)	
426.8	+			$8^+ \rightarrow 6^+$ ^{154}Gd	a)	
434.5		+	+	$15/2^- \rightarrow 13/2^-$ ^{193}Tl	b)	
451.5		+	+	partly $4^{+*} \rightarrow 2^+$ ^{198}Pt	e)	
454	+	+		^{196}Pb	h)	+
477.6		+	+	^{193}Hg	c)	
494	+			$10^+ \rightarrow 8^+$ ^{154}Gd	a)	
507	+	+		^{198}Pb	h)	+
511	+	+	+	annihilation e^+e^-		
535		+	+	^{193}Hg	c)	
540	+	+		^{197}Pb	h)	+
547.7	+			$12^+ \rightarrow 10^+$ ^{154}Gd	a)	
555		+	+	radioactivity ^{197}Hg	c)	
563.1		+	+	^{197}Hg	c)	
579.7		+	+	^{198}Pt	e)	
597.9		+	+	$2^{+*} \rightarrow 0^+$ ^{193}Hg	f)	
606.1		+	+	$(13/2^- \rightarrow 11/2^-)$ ^{193}Tl	b)	
614.2		+	+	^{193}Hg	c)	
615.3		+	+	$(4^{+*} \rightarrow 2^+)$ $^{198}Hg+(0^{+*} \rightarrow 2^+)$ ^{198}Pt	e)	
639.0		+	+	^{193}Hg	c)	
658		+	+	radioactivity		
676.4	+			$4^+ \& 4^+$ ^{154}Gd	a)	
690		+		$0^{+*} \rightarrow 0^+$ $^{72}Ge(n,n')$	h)	
713.2		+	+	$13/2^- \rightarrow 9/2^-$ ^{193}Tl	b)	
730.9		+	+	$6^+ \rightarrow 4^+$ ^{199}Hg	f,g)	
773	+	+		^{198}Pb	h)	+
838		+	+	radioactivity		
839.1		+	+	$5^- \rightarrow 4^+$ ^{199}Hg	f)	
875	+			$(2^+ \rightarrow 2^+)$ ^{154}Gd	a)	
884	+			$(4^+ \rightarrow 4^+)$ ^{154}Gd	a)	
910		+	+	radioactivity		
997	+			$2^+ \rightarrow 0^+$ ^{154}Gd	a)	
1005	+			$3^{+*} \rightarrow 2^+$ ^{154}Gd	a)	
1142	+			$6^+ \rightarrow 4^+$ ^{154}Gd	a)	
1268		+	+	radioactivity		
1295		+	+	radioactivity		

gates (keV) \ lines in coincidence (keV)	69	74.2 XK_α Pb	85.4 XK_β Pb	191	464	501.7	503	564	599	852
69	-	+	+	+	+	+	+	-	-	+
74.2 XK_α Pb	+	(+)	+	+	+	+	+	(+)	(+)	+
85.4 XK_β Pb	(+)	(+)	(+)	+	(+)	+	+	(+)	(+)	(+)
191	+	+	+	-	+	+	+	-	-	+
464	(+)	(+)	(+)	+	-	+	+	-	-	+
501.7	(+)	(+)	(+)	+	+	(-)	+	+	(+)	+
503	(+)	(+)	+	+	+	+	(-)	-	-	+
564	-	(+)	(+)	-	-	+	-	-	+	+
599	-	(+)	(+)	-	-	+	(-)	+	-	+
852	+	+	+	+	+	+	+	+	+	-

Table 6. Delayed coincidences results for the set of lines assigned to ^{192}Pb.

Multipolarity	α_T (Ref.22)
E1	0.26
M1	5.51
E2	37.1
M2	178

Table 7. Total conversion coefficients for the 69 keV transition according to various possible multipolarities.

Nucleus	Transition	E_γ(keV)	α_T (ref.22)	Calculated γ-branching ratio $\frac{IE1}{IE2}$
$^{194}_{Pb}$	$10^+ \xrightarrow{E1} 9^-$	173.5	.114	29.2
	$(10^+ \xrightarrow{E2} 8^+)$	≳ 64	59.26	
$^{192}_{Pb}$	$10^+ \xrightarrow{E1} 9^-$	69	0.26	2.1
	$(10^+ \xrightarrow{E2} 8^+)$	64	59.26	
	$(8^+ \xrightarrow{E1} 7^-)$	196	$7.54\ 10^{-2}$	0.03
	$8^+ \xrightarrow{E2} 6^+$	599	$1.64\ 10^{-2}$	
	$6^+ \xrightarrow{E1} 5^-$	61	$3.7\ 10^{-1}$	$1.5\ 10^{-3}$
	$6^+ \xrightarrow{E2} 4^+$	564	$1.9\ 10^{-1}$	
	$(7^- \xrightarrow{E1} 6^+)$	403	$1.58\ 10^{-2}$	0.97
	$7^- \xrightarrow{E2} 5^-$	464	$3.82\ 10^{-2}$	

Table 8. Estimation of the γ-ray branching ratios $\frac{I(E1)}{I(E2)}$ for E1 and E2 transitions from selected nuclear states in $^{194-192}_{Pb}$. Parentheses are for unobserved transitions. The adopted values for B(E1,E2) are extracted from the corresponding measured quantities for the respective $5^- \xrightarrow{E1} 4^+$ and $12^+ \xrightarrow{E2} 10^+$ transitions in the heavier isotopes (see text).

Gates (keV) \ Lines in coincidence (keV)	338	454	507	540	773
338	+	+	+	+	+
454	+	–	+	+	+
507	+	+	+	+	+
530	+	+	+	–	+
773	+	+	+	+	–

Table 9..Delayed coincidences results for the set of lines assigned to ^{190}Pb.

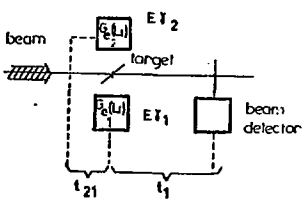

Fig. 1.

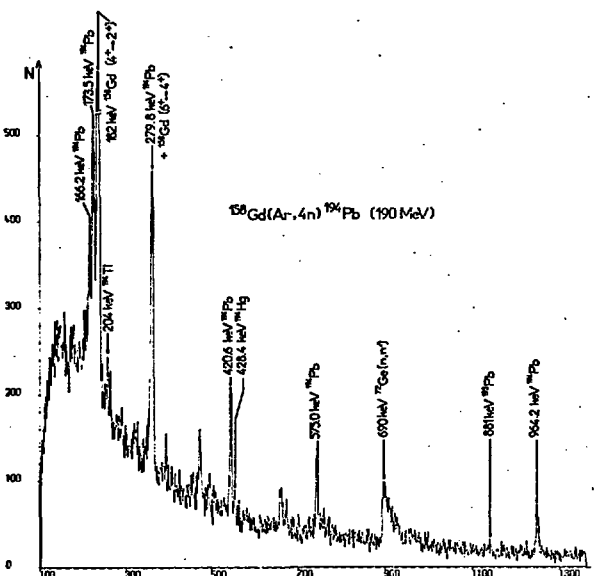
N
500
400
300
200
100
0
100
300
500
700
900
1100
1300
CHANNELS
^{158}Gd(Ar,4n)^{194}Pb (190 MeV)
160.9 keV ^{194}Pb
173.1 keV ^{194}Pb
182 keV ^{154}Gd (6$^+$→4$^+$)
204 keV ^{194}Tl
279.8 keV ^{194}Pb
+ ^{154}Gd (8$^+$→6$^+$)
420.6 keV ^{194}Pb
428.4 keV ^{194}Hg
573.0 keV ^{194}Pb
690 keV ^{72}Ge(n,n')
881 keV ^{194}Pb
964.2 keV ^{194}Pb

Fig.2.

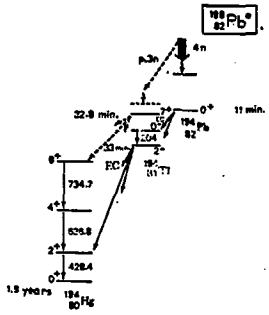
198 82 Pb*
4n
p,3n
32.8 min.
11 min.
194 82 Pb
EC
734.7
525.8
428.4
1.5 years
194 80 Hg

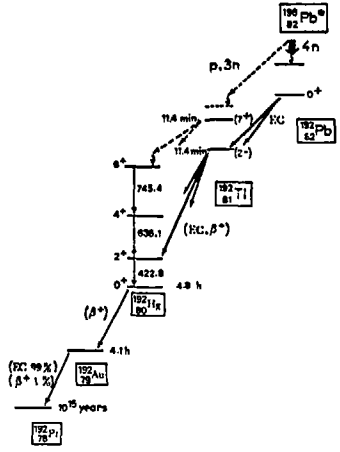
196 82 Pb*
4n
p,3n
11.4 min
EC
192 82 Pb
743.4
636.1
422.8
192 81 Tl
(EC,β+)
4.8 h
192 80 Hg
(β+)
4.1h
(EC: 99 %)
(β+ 1 %)
192 79 Au
10^15 years
192 78 Pt

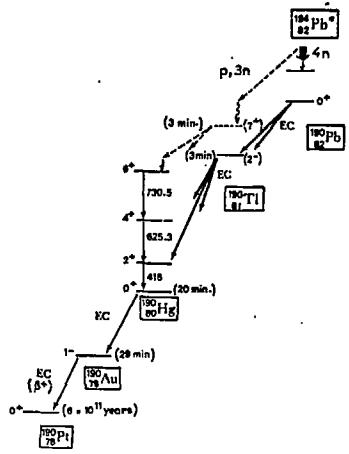
194 82 Pb*
4n
p,3n
(3 min.)
EC
190 82 Pb
(3min)
730.5
625.3
416
190 81 Tl
(20 min.)
190 80 Hg
EC
(29 min)
EC
(β+)
190 79 Au
(6 x 10^11 years)
190 78 Pt

Fig.3.

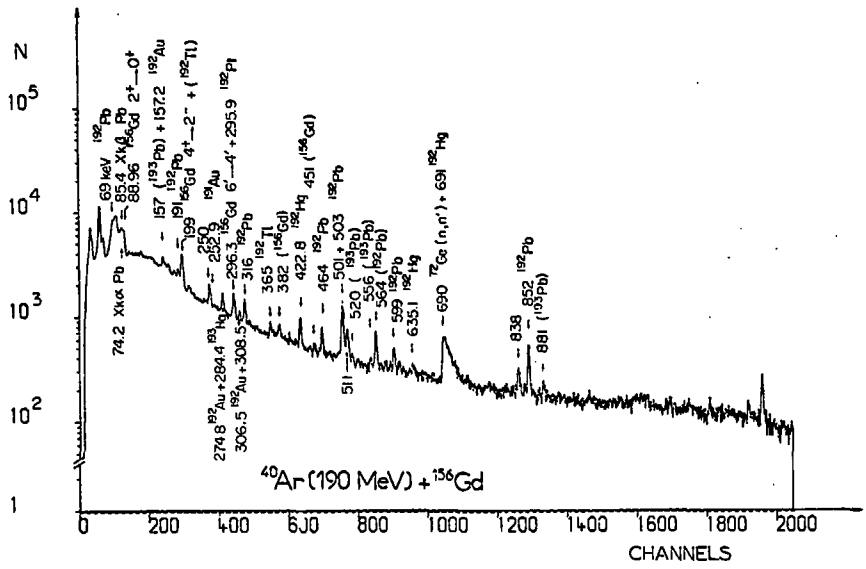
N
10^5
10^4
10^3
10^2
1
0
200
400
600
800
1000
1200
1400
1600
1800
2000
CHANNELS
^{40}Ar (190 MeV) + ^{156}Gd
69 keV ^{192}Pb
74.2 Xkα Pb
85.4 Xkα Pb
88.96 ^{156}Gd 2$^+$—0$^+$
157 (^{193}Pb) + 157.2 ^{192}Au
191 ^{195}Pb
199 ^{156}Gd 4$^+$—2$^-$ + (^{192}Tl)
250
252.9
^{191}Au
274.8 ^{192}Au + 284.4 ^{193}Hg
296.3 ^{156}Gd 6$^-$—4$^+$ + 295.9 ^{192}Pt
306.5 ^{192}Au + 308.5
316 ^{192}Pb
365 ^{192}Tl
382 (^{156}Gd)
422.8 ^{192}Hg
451 (^{156}Gd)
464 ^{192}Pb
501 + 503 ^{192}Pb
511
520 (^{193}Pb)
556 (^{192}Pb)
564 (^{192}Pb)
599 ^{192}Pb
635.1 ^{192}Hg
690 ^{72}Ge (n,n') + 691 ^{192}Hg
838
852 ^{192}Pb
881 (^{193}Pb)

Fig.4a.

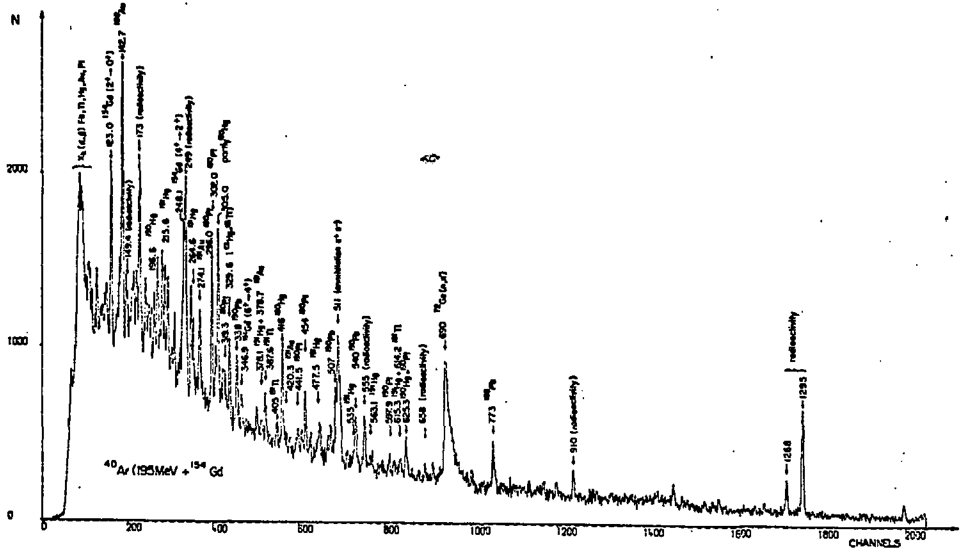
N
CHANNELS
^{40}Ar (195MeV + ^{154}Gd
0
1000
2000
200
400
600
800
1200
1400
1600
1800
2000
123.0 ^{154}Gd (2⁺→0⁺)
142.7 ^{189}Au
149.4 (radioactivity)
173 (radioactivity)
196.6 ^{190}Hg
215.6 ^{191}Hg
248.1 ^{154}Gd (4⁺→2⁺)
249 (radioactivity)
264.6 ^{191}Hg
274.1 ^{191}Au
296.0 ^{190}Pt
302.0 ^{190}Pt
305.0 partly ^{190}Hg
329.6 (^{191}Hg+^{191}Tl)
346.9 ^{154}Gd (6⁺→4⁺)
378.1 ^{191}Hg + 378.7 ^{191}Au
387.6 ^{191}Tl
405 ^{191}Tl
416 ^{190}Hg
420.3 ^{191}Au
441.5 ^{190}Pt
454 ^{190}Pt
477.5 ^{191}Hg
507 ^{190}Pb
511 (annihilation e⁺ e⁻)
535 ^{191}Hg
540 ^{190}Pb
555 (radioactivity)
563.1 ^{191}Hg
587.9 ^{190}Pt
615.3 ^{191}Hg + 614.2 ^{191}Tl
625.3 ^{190}Hg + ^{190}Pt
658 (radioactivity)
690 ^{72}Ge (n,n')
773 ^{190}Pb
910 (radioactivity)
1268
1295
radioactivity

Fig.45.

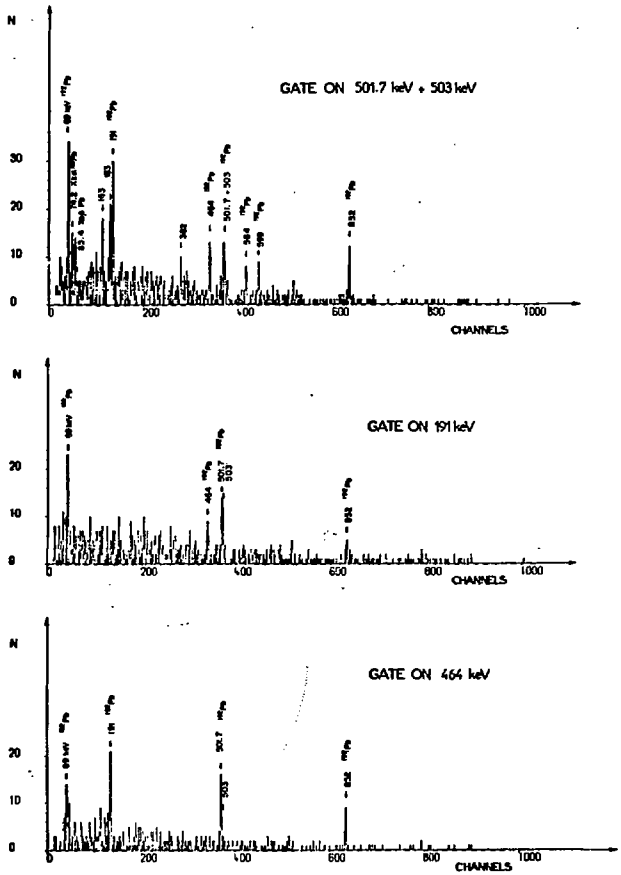
N
GATE ON 501.7 keV + 503 keV
30
20
10
0
0
200
400
600
800
1000
CHANNELS
N
GATE ON 191 keV
20
10
0
0
200
400
600
800
1000
CHANNELS
N
GATE ON 464 keV
20
10
0
0
200
400
600
800
1000
CHANNELS

Fig.5.

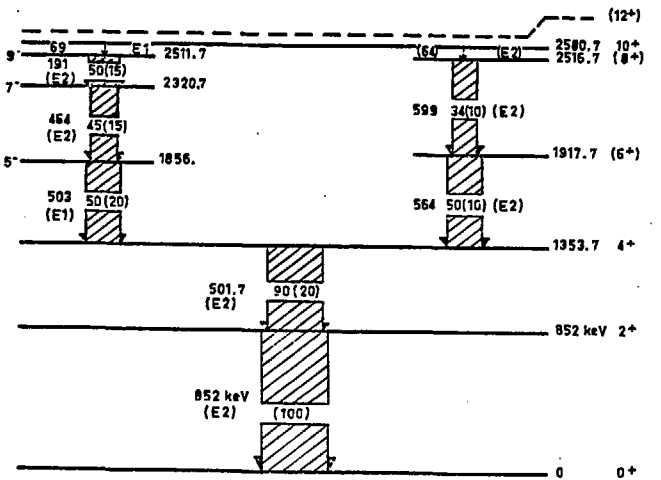
(12+)
69
E1
2511.7
9-
191
(E2)
50(15)
7-
2320.7
464
(E2)
45(15)
5-
1856.
503
(E1)
50(20)
(60)
(E2)
2580.7 10+
2516.7 (8+)
599 34(10) (E2)
1917.7 (6+)
564 50(10) (E2)
1353.7 4+
501.7
(E2)
90(20)
852 keV 2+
852 keV
(E2)
(100)
0 0+
192 Pb

Fig.6.

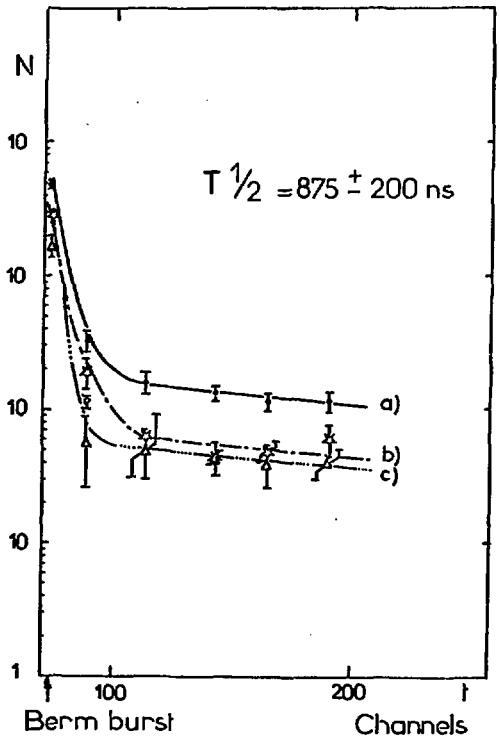

Fig. 7.

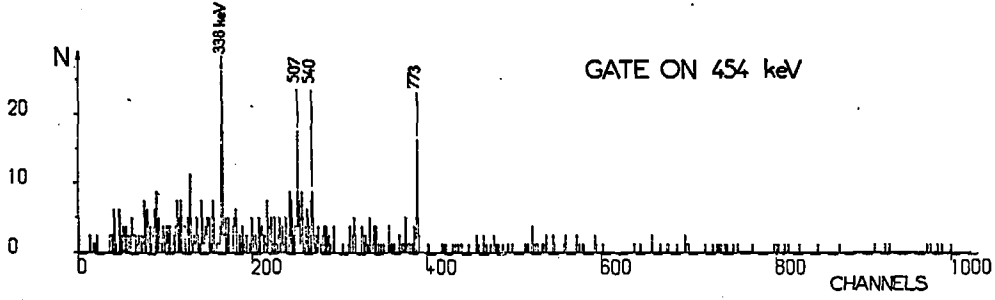
N
338 keV
507
540
773
GATE ON 454 keV
20
10
0
0
200
400
600
800
1000
CHANNELS

Fig.8.

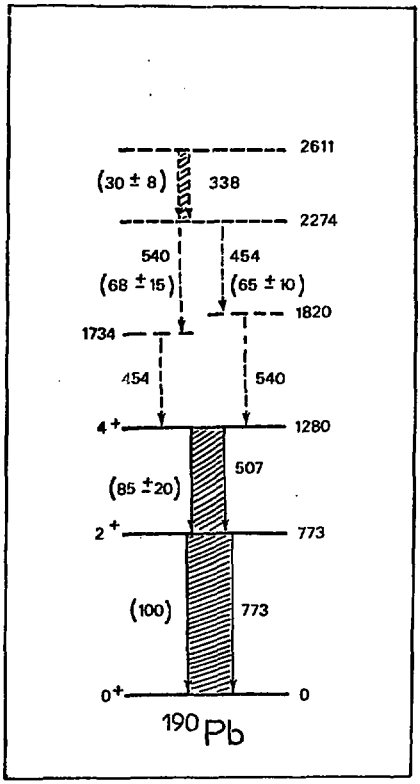
2611
(30 ± 8)
338
2274
540
(68 ± 15)
454
(65 ± 10)
1820
1734
454
540
4+
1280
507
(85 ± 20)
2+
773
(100)
773
0+
0
190Pb

Fig.9.

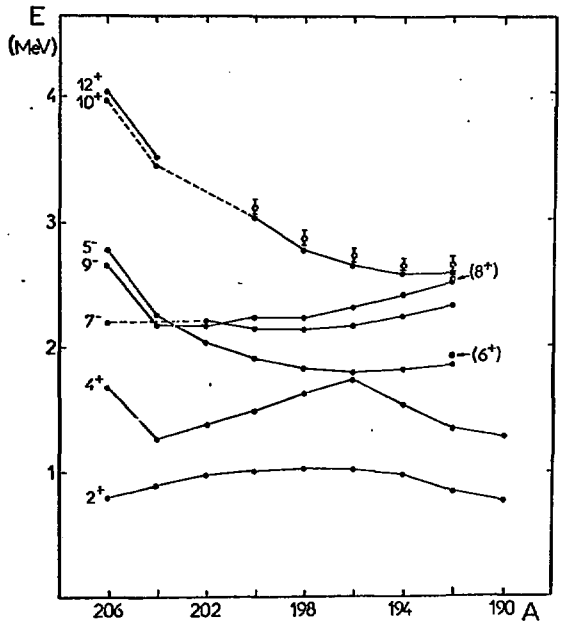

Fig. 10.

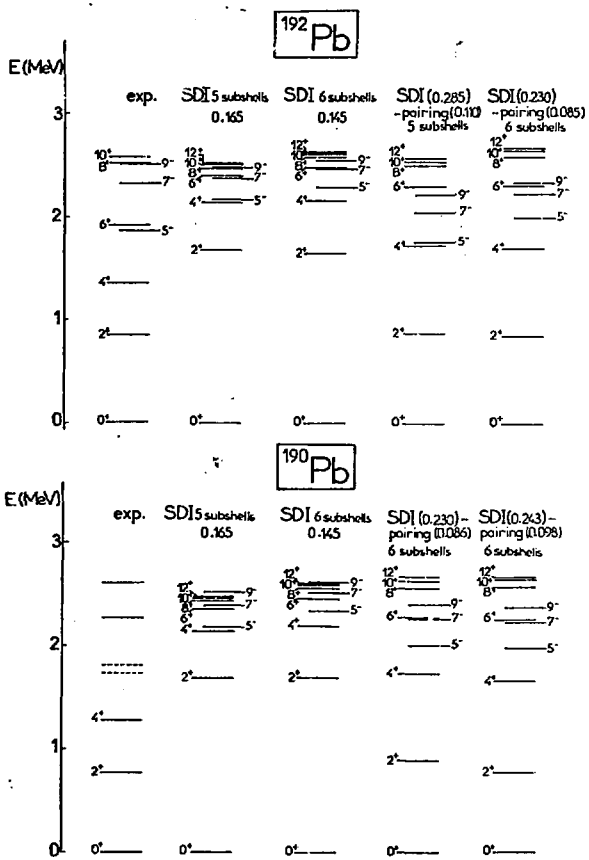
192Pb
E(MeV)
exp.
SDI 5 subshells 0.165
SDI 6 subshells 0.145
SDI (0.285) -pairing(0.110) 5 subshells
SDI(0.230) -pairing (0.085) 6 subshells
190Pb
E(MeV)
exp.
SDI 5 subshells 0.165
SDI 6 subshells 0.145
SDI (0.230) - pairing (0.086) 6 subshells
SDI(0.243) - pairing (0.098) 6 subshells

Fig. 11.

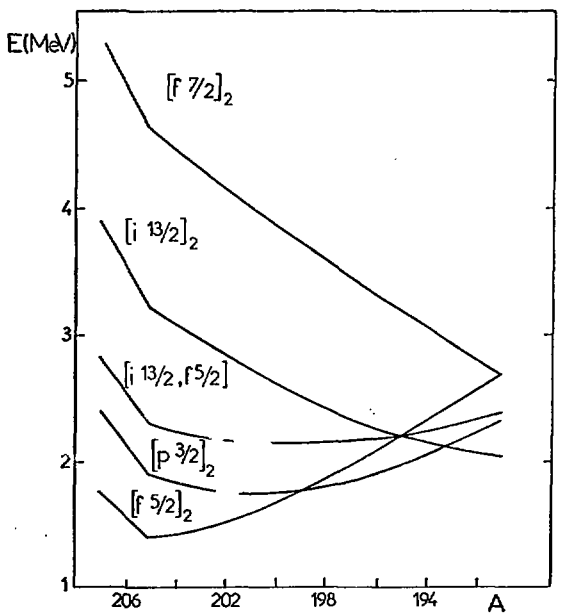

Fig. 12.

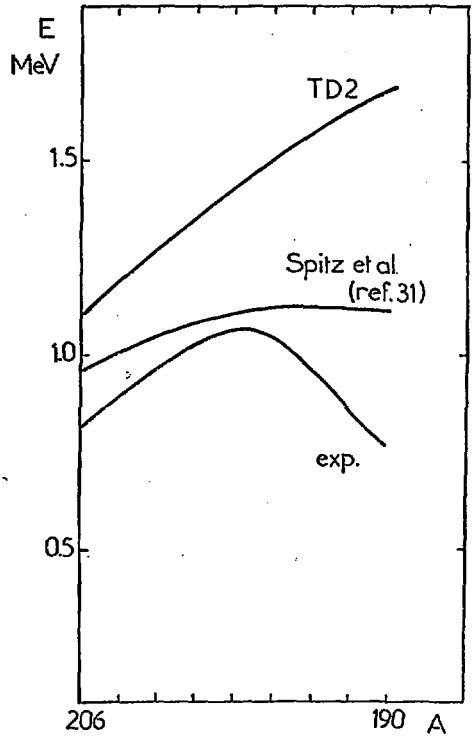

Fig. 13.